Electronic Supplementary Material (ESI) for Inorganic Chemistry Frontiers.

Supporting Information

Exploring the Evolution Process of High-Performance Amethyst Geode-Shaped Hollow Spherical $LiFePO_4$

Lu Chen,[a,1] Yan Meng,[b,1] Yujue Wang,[a] Pengfei Wang,[b] Jianming Li,[b] Qinniu Lv,[c] Zhaokun Zhang,[d] Qian Zhao,[e] and Dan Xiao[a,b,d,*]

Experimental section

Synthesis of LFP with longer calcination time

Apart from calcination temperature maintenance at 650°C for 8 h, other conditions were unchanged correlated with A-LFP-650, noted as A-LFP-650-8.

Synthesis of LFP with different calcination temperatures

Experimental conditions remain unchanged related to A-LFP-650, except adjustment the calcination temperature. After temperature maintained at 350°C for 3 h, materials were sintered at 600°C and 700°C for 4 h, denoted as A-LFP-600, A-LFP-700, respectively.

Synthesis of LFP with longer ball milling time

Excepting rise ball milling time up to 4 h and 6 h, other conditions are consistent with A-LFP-650, named as A-LFP-4-650, A-LFP-6-650.

Synthesis of LFP with single carbon source

Additional glucose and PEG 6000 serve as single carbon source respectively, called A-LFP-G, A-LFP-PEG. Other conditions keep unchanged.

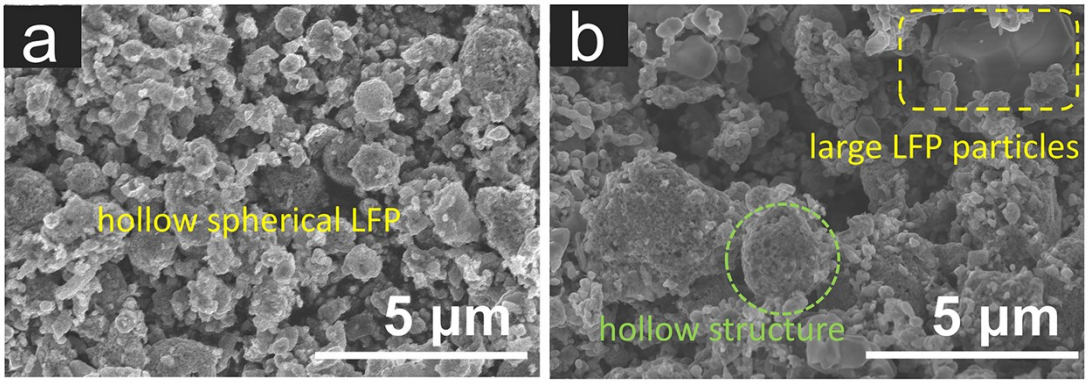

Fig. S1 SEM images of (a) A-LFP-650, (b) A-LFP-650-8. Hollow spherical structure emerged both in A-LFP-650 and A-LFP-650-8. Yet longer calcination time form larger LFP particles, as marked in Fig. S1b.

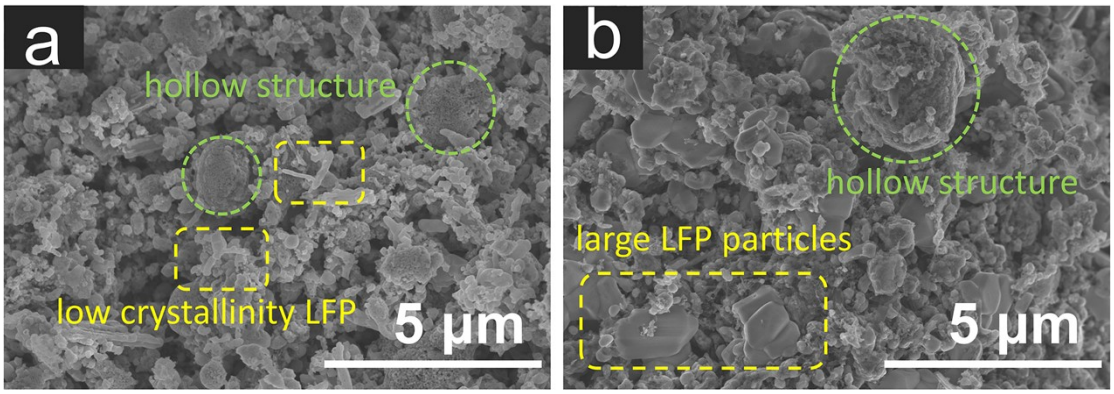

Fig. S2 SEM images of LFP samples at different calcination temperature: (a) A-LFP-600, (b) A-LFP-700. Morphology exhibits that A-LFP-600 consists of porous hollow spheres and disorderly arrangement of fine LFP crystals. A-LFP-700 also involves porous hollow spheres but enclosed with large LFP crystals. This result shows that calcination temperature has influence on crystallinity and particle size, but has no obvious effect on the porous spherical structure.

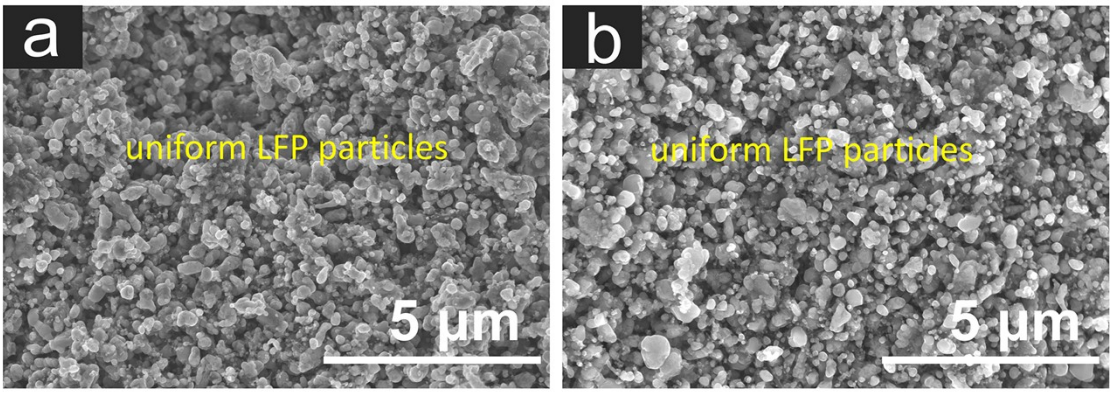

Fig. S3 SEM images of materials with longer ball milling time: (a) A-LFP-4-650, (b) A-LFP-6-650. As the time of ball milling increases, LFP with uniform particles formed, but no hollow spheres are observed.

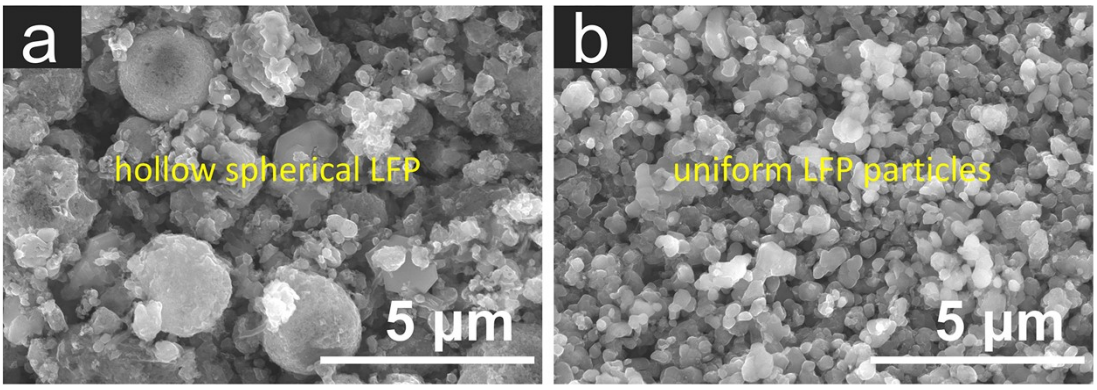

Fig. S4 SEM images of single carbon source LFP materials. (a) A-LFP-G, (b) A-LFP-PEG. PEG as single carbon source is hardly to maintain spherical structure, illustrating glucose was primary agent connected to spherical template as a result of sufficient hydroxyl groups.

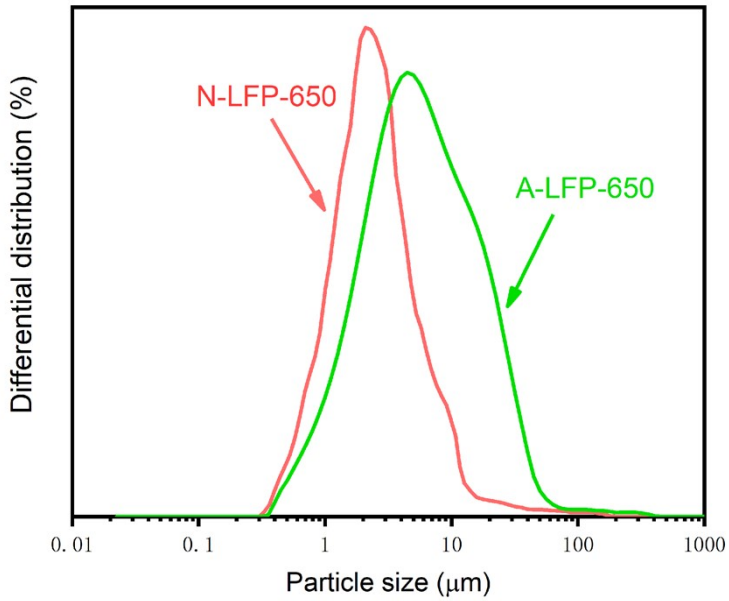

Fig. S5 Particle size distribution (PSD) of A-LFP-650 and N-LFP-650. N-LFP-650 exhibits a narrower PSD.

Fig. S6 Photographs of pure APP after calcined at low temperature.

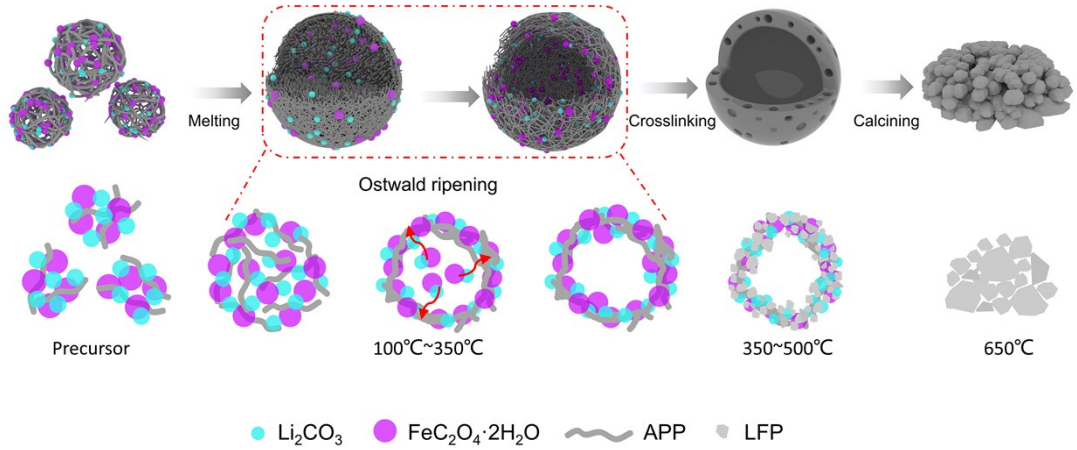

Scheme S1 The formation process of n-A-LFP-650. Due to the lack of carbon source, the shaped hollow-spherical structure originated from APP during low-temperature (<350°C) calcination cannot be maintained in the final product (>500°C).

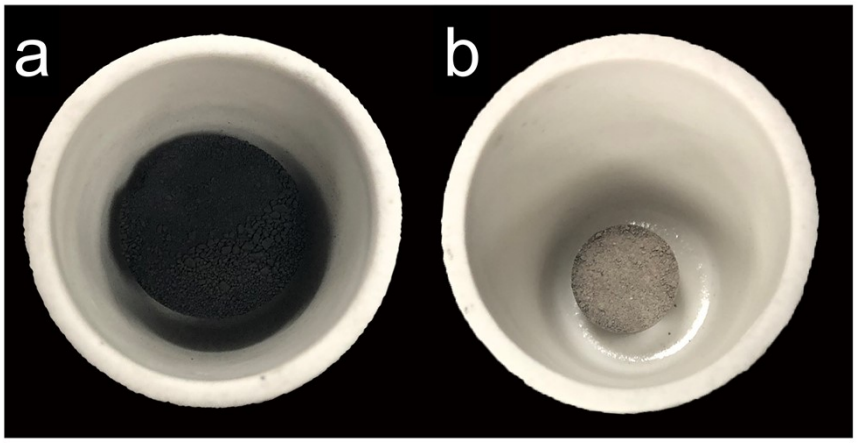

Fig. S7 Photographs of products after calcined at 650°C (a)A-LFP-650, (b)n-A-LFP-650.

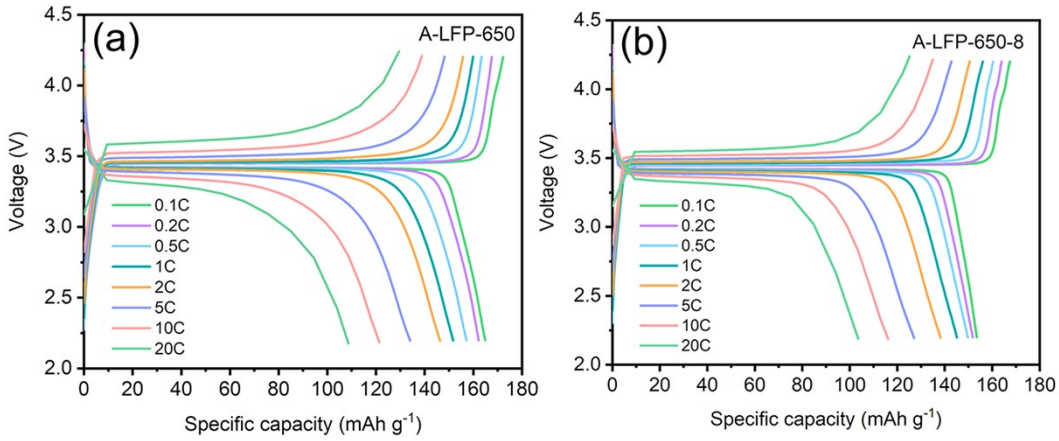

Fig. S8 Rate performance at 0.1~20 C of (a) A-LFP-650, (b) A-LFP-650-8. GCD curve of A-LFP-650-8 shows a satisfying rate performance behavior like A-LFP-650, but presents a decline of capacity at low discharge rate.

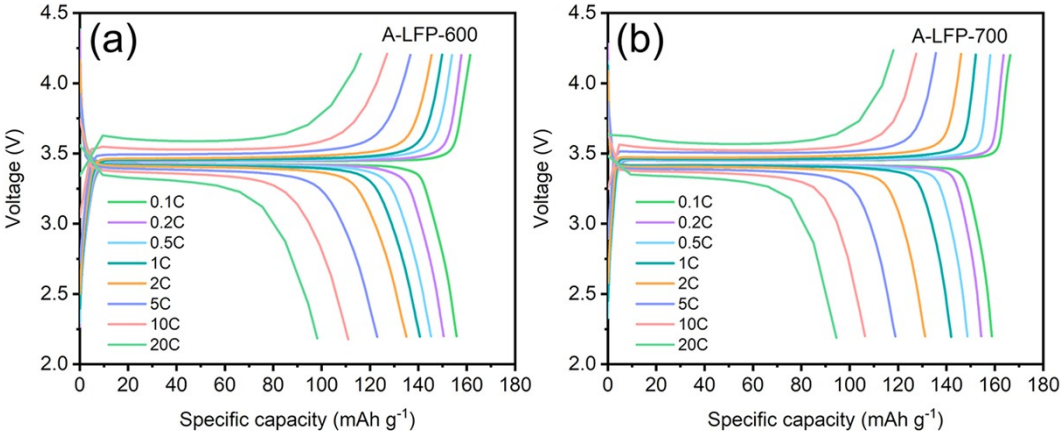

Fig. S9 GCD curves of (a) A-LFP-600, (b) A-LFP-700. Both A-LFP-600 and A-LFP-700 exhibit inferior rate performance, illustrating that large-sized crystal and low crystallinity LFP particles are unfavorable for electrochemical performance.

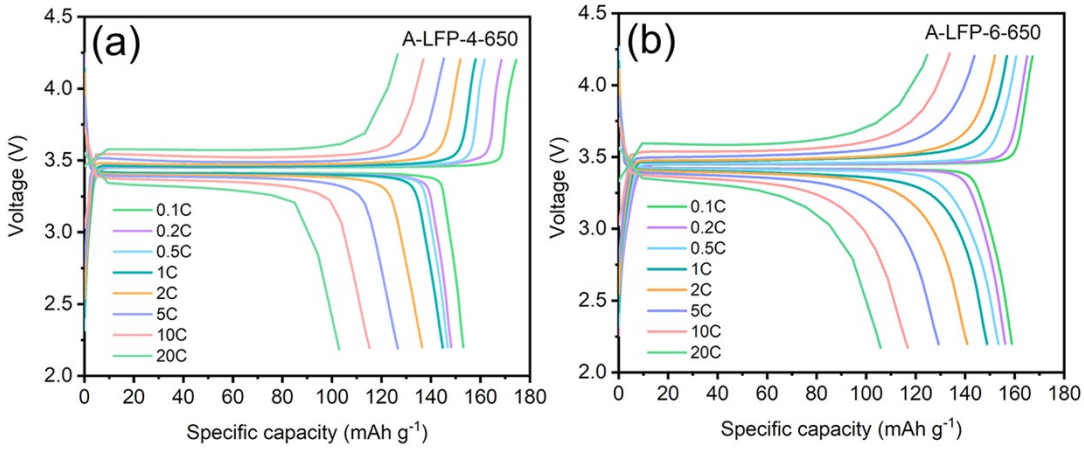

Fig. S10 Electrochemical performance of (a) A-LFP-4-650, which shows a drop of energy efficiency; (b) A-LFP-6-650.

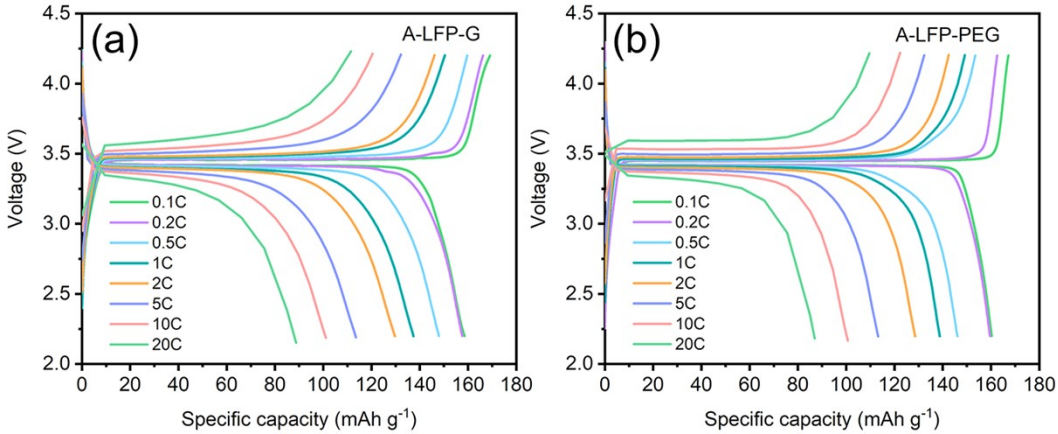

Fig. S11 GCD curves of (a)A-LFP-G, (b) A-LFP-PEG. $LiFePO_4$ materials with single carbon source possesses inferior rate performance.

Table S1
Capacity values of samples at various discharge rates.

Sample	Capacity (mAh g^{-1})								Polarization at 0.1 C (mV)
	0.1 C	0.2 C	0.5 C	1 C	2 C	5 C	10 C	20 C	
A-LFP-650	163	161	158	153	146	134	123	110	28
A-LFP-650-8	154	151	149	144	138	127	116	103	29
A-LFP-600	155	150	145	140	135	122	110	98	28
A-LFP-700	158	154	148	141	131	118	106	96	33
A-LFP-4-650	153	148	146	144	136	126	115	102	37
A-LFP-6-650	158	156	153	148	140	129	116	105	33
A-LFP-G	158	157	148	137	130	113	101	89	36
A-LFP-PEG	160	159	146	139	128	113	100	87	29

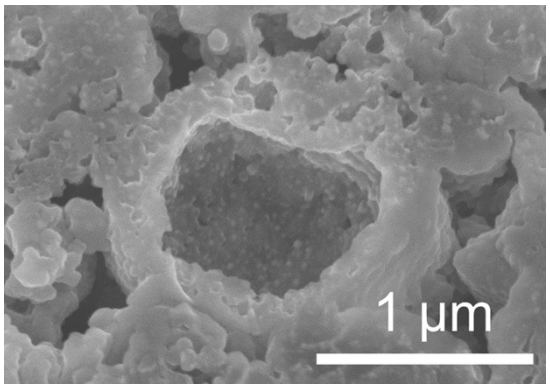

Fig. S12 Cross-sectional view of A-LFP-650 electrode after 200 cycles at 10 C. The hollow spherical structure maintains well after cycling in A-LFP-650 cathode.

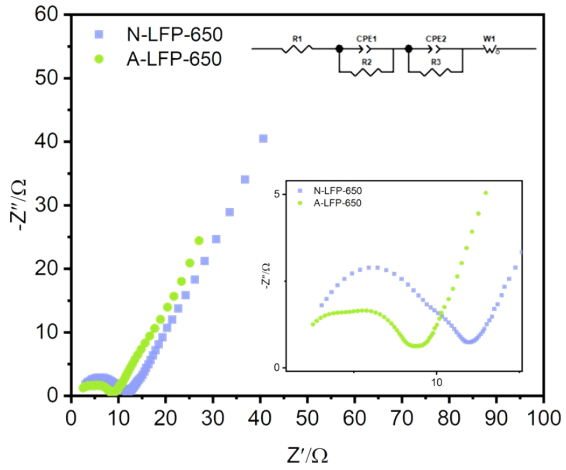

Fig. S13 Nyquist plots of A-LFP-650 and N-LFP-650 after 200 cycles at 10 C.

Compared to EIS data after first charge, R_{SEI} and R_{ct} values of A-LFP-650 and N-LFP-650 both decreased after 200 cycles, implying stable interface formed during cycling and the electrochemical kinetics did not deteriorate obviously. EIS results are in accordance with rate performance and cycling performance.

Table S2

Impedance values for A-LFP-650 and N-LFP-650 after 200 cycles.

Sample	R_S/Ω	R_{SEI}/Ω	R_{ct}/Ω
A-LFP-650	1.152	3.637	2.981
N-LFP-650	1.335	5.327	5.946

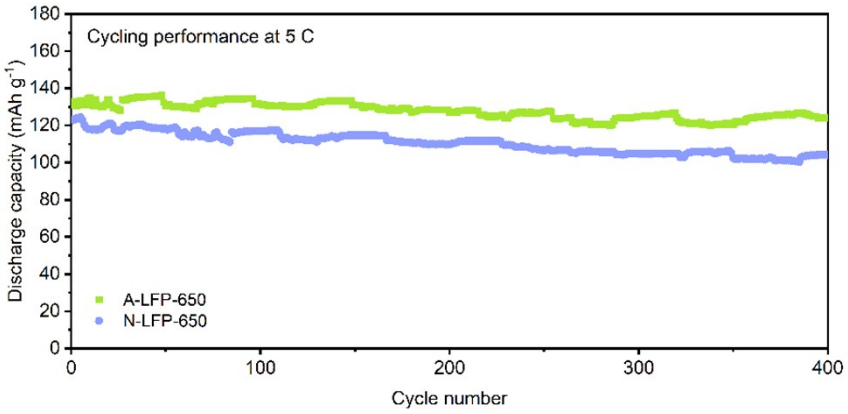

Fig. S14 Cycling performance of A-LFP-650 and N-LFP-650 at 5 C. After A-LFP-650 After 400 cycles at 5 C, the retention capacity of A-LFP-650 is 92%, while this of N-LFP-650 is 84%.

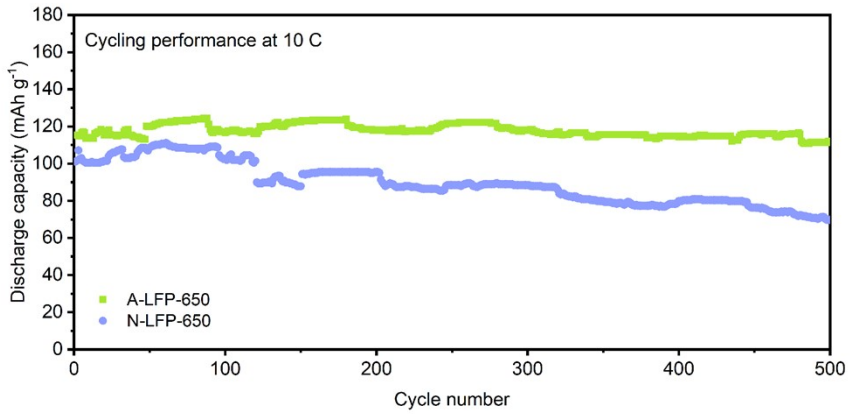

Fig. S15 Cycling performance of A-LFP-650 and N-LFP-650 at 10 C.
After 500 cycles at 10 C, the retention capacity of A-LFP-650 is 90%, while this of N-LFP-650 is 64%.

Table S3

Loading density of A-LFP-650.

	A-LFP-1	A-LFP-2	A-LFP-3	A-LFP-4	A-LFP-5
Loading mass (mg)	7.94	7.42	8.01	7.64	7.56
Thickness (μm)	30	28	31	30	30
Loading density (g/cm^3)	1.72	1.72	1.68	1.65	1.64

Loading density (ρ, g/cm^3) is observed from equations of $\rho = m/v$ and $v = \pi R^2 H$, where m is loading mass (mg), R is the radius of electrodes (R = 7 mm), H represents the thickness of electrodes (μm).

Table S4

Loading density of commercial LFP material.

	C-LFP-1	C-LFP-2	C-LFP-3	C-LFP-4	C-LFP-5
Loading mass (mg)	7.48	6.02	8.68	7.29	7.84
Thickness (μm)	27	22	31	28	27
Loading density (g/cm^3)	1.80	1.77	1.82	1.69	1.89